PNAS RESEARCH ARTICLE | BIOCHEMISTRY OPEN ACCESS

ASPM promotes ATR-CHK1 activation and stabilizes stalled replication forks in response to replication stress

Xingxuan Wu[a,c,d,1], Shibin Xu[a,b,1], Peipei Wang[a], Zhao-Qi Wang[d], Hongxiang Chen[a], Xingzhi Xu[a,c,2,3], and Bin Peng[a,3]

Edited by Lorraine Symington, Columbia University Irving Medical Center, New York, NY; received March 3, 2022; accepted August 23, 2022

ASPM is a protein encoded by *primary microcephaly 5* (*MCPH5*) and is responsible for ensuring spindle position during mitosis and the symmetrical division of neural stem cells. We recently reported that ASPM promotes homologous recombination (HR) repair of DNA double strand breaks. However, its potential role in DNA replication and replication stress response remains elusive. Interestingly, we found that ASPM is dispensable for DNA replication under unperturbed conditions. However, ASPM is enriched at stalled replication forks in a RAD17-dependent manner in response to replication stress and promotes RAD9 and TopBP1 loading onto chromatin, facilitating ATR-CHK1 activation. ASPM depletion results in failed fork restart and nuclease MRE11-mediated nascent DNA degradation at the stalled replication fork. The overall consequence is chromosome instability and the sensitization of cancer cells to replication stressors. These data support a role for ASPM in loading RAD17-RAD9/TopBP1 onto chromatin to activate the ATR-CHK1 checkpoint and ultimately ensure genome stability.

DNA replication | ATR-CHK1 | replication stress | primary microcephaly

Significance

ASPM (encoded by *MCPH5*) is a frequently mutated protein, and such mutations occur in >40% of cases of primary microcephaly (MCPH). Here, we characterize a function of ASPM in DNA replication and the replication stress response. ASPM serves as a scaffold to load stimulators required for ATR-CHK1 checkpoint signaling upon replication stress, which protects stalled replication forks from degradation. ASPM deficiency leads to genomic instability and the sensitization of cancer cells to replication stressors.

During neurogenesis, neural stem cells undergo a sequence of proliferation, migration, and differentiation (1). Should neurogenesis be hindered, perhaps due to a low number of neuroprogenitor cells, severe neurological conditions such as microcephaly can ensue. Microcephaly is a rare disorder characterized by small brain size and mental retardation (2, 3). There are two clinical subtypes: primary microcephaly (PM) and secondary microcephaly (SM) (4). So far, mutations in 25 pathogenic genes (MCPH1-25) associated with PM have been identified (3). These genes have varied roles, ranging from cell cycle checkpoint activation to DNA repair activities (5, 6). ASPM (encoded by *MCPH5*) is the most frequently mutated of these proteins and is known to underlie >40% of MCPH cases (7). ASPM functions in centriole duplication, spindle orientation, and organization (8), but can also localize to the spindle pole (9) and regulate mitosis by organizing microtubules (10). In addition, ASPM functions during meiosis and acts as a positive regulator of Wnt signaling (11–13). Furthermore, patients with *MCPH5* mutations exhibit reduced numbers of neuroprogenitor cells during brain development, which indicates defects in control of symmetric/asymmetric divisions and/or in DNA replication. However, the involvement of ASPM in the DNA replication and/or replication stress response is currently unknown.

The DNA replication machinery comprises various proteins, including DNA polymerases, DNA helicase complexes, and various other auxiliary proteins that together ensure accurate genome replication once every cell cycle (14). Any factors that affect replication fork stability or fork restart, and thus cause DNA replication stress, risk disturbing genome stability (15) and promoting cancer development. Ataxia-telangiectasia and Rad3-related (ATR) kinase, which is a member of the phosphoinositide 3-kinase-related kinases (PIKKs) family (16, 17), is essential for sensing replication stress and signal transduction (18, 19). ATR works together with CHK1 in a signaling pathway that serves to safeguard against DNA damage and to prevent incompletely replicated cells from entering mitosis under conditions of replication stress (20–25). When replication forks stall, single-stranded DNA (ssDNA) is exposed. The heterotrimeric protein complex RPA coats ssDNA (26, 27) and then recruits the RAD17, 9-1-1 complex, and TopBP1 to activate ATR (28–34). ATR subsequently activates CHK1 to facilitate the restarting of the DNA replication fork (24, 35). Various proteins assist with fork reconstruction and reversed fork (RVF) formation (36). In particular, RAD51 replaces RPA (37) and initiates fork reversal with the help of replication fork remodeling proteins. Once replication stress is lifted, the replication fork will restart (38, 39). However, if the stress persists, the replication fork will collapse, leading to one-ended double strand breaks (DSBs) (40, 41).

Throughout this process, it's critical that nascent DNA exposed at stalled replication forks is protected from nucleolytic degradation by promiscuous nucleases, such as

Author affiliations: [a]The Sixth Affiliated Hospital of Shenzhen University, Guangdong Key Laboratory for Genome Stability and Disease Prevention and Carson International Cancer Center, Marshall Laboratory of Biomedical Engineering, Shenzhen University School of Medicine, Shenzhen 518060, China; [b]Guangdong Key Laboratory for Biomedical Measurements and Ultrasound Imaging, Shenzhen University, Shenzhen 518060, China; [c]Shenzhen University–Friedrich Schiller Universität Jena Joint PhD Program in Biomedical Sciences, Shenzhen University School of Medicine, Shenzhen 518060, China; and [d]Laboratory of Genome Stability, Leibniz Institute on Aging–Fritz Lipmann Institute, Jena 07745, Germany

Author contributions: X.X. and B.P. designed research; X.W., S.X., P.W., and B.P. performed research; X.W., S.X., P.W., Z.-Q.W., H.C., X.X., and B.P. analyzed data; and X.X. and B.P. wrote the paper.

The authors declare no competing interest.

This article is a PNAS Direct Submission.

[1]X.W. and S.X. contributed equally to this work.

[2]Lead contact.

[3]To whom correspondence may be addressed. Email: Xingzhi.Xu@szu.edu.cn or binpeng@szu.edu.cn.

This article contains supporting information online at http://www.pnas.org/lookup/suppl/doi:10.1073/pnas.2203783119/-/DCSupplemental.

Published September 26, 2022.

EXO1, DNA2, and MRE11 (42–45). CtIP, for example, prevents DNA2–WRN-dependent nascent degradation at stalled forks in the absence of BRCA1 (42, 46).

In this study, we aimed to determine a potential role for ASPM in DNA replication and/or the replication stress response. To this end, we established ASPM knockout (KO) and FLAG-GFP-ASPM knockin (KI) cell lines (47). We used these to determine whether and how ASPM might be involved in replication stress–induced ATR-CHK1 activation, replication fork stabilization, and protection from nucleolytic degradation.

Results

ASPM Associates with DNA Replication Factors to Mediate DNA Replication. To understand the biological function of ASPM, we sought to identify its interacting networks through immunoprecipitation combined with mass spectrometric analysis. We generated rabbit polyclonal antibodies against 16 peptides spanning all major regions of ASPM but found no single antibody suitable for immunoprecipitation and only one antibody (BL1615) suitable for immunoblotting and immunofluorescence analysis (9, 47). We then turned to the ASPM KI cell line, in which the FLAG-GFP cassette is inserted in frame before the first start codon in ASPM by CRISPR-Cas9 technology in HeLa cells as previously described (47). Two monoclonal populations of ASPM KI HeLa cells exhibited a GFP signal enriched at the spindle poles (*SI Appendix*, Fig. S1*A* and Dataset S1). We performed affinity purification of the FLAG-GFP-ASPM immunocomplex followed by silver staining (Fig. 1*A*). Subsequent mass spectrometry identified ASPM along with the RFC complex subunits (RFC1-5), BRCA2 (which protects stalled replication forks), and MCM5, a core subunit of the MCM complex (Fig. 1*B*).

The pentameric RFC opens the sliding clamp and loads it onto the DNA chain (48). It also forms a complex with RAD17, which replaces RFC1, during the genotoxic stress response to load the RAD9-HUS1-RAD1 (9-1-1) complex onto DNA at sites of damage and/or stalled replication forks (28, 30). Interestingly, our coimmunoprecipitation assays confirmed that endogenous RFC1, RFC2, RFC5, RAD17, and TopBP1 were present in the FLAG-GFP-ASPM immunocomplex (Fig. 1*C*). To rule out the possibility that their interaction was bridged by DNA, coimmunoprecipitation assays were perform in the presence or absence of the nuclease benzonase, and the results revealed that benzonase treatment did not disrupt these interactions (*SI Appendix*, Fig. S1*B*). This indicated that the interaction between ASPM and the identified replication factors was DNA independent.

Given that ASPM seems to physically associate with DNA replication factors, we reasoned that ASPM would likely have a role in DNA replication. To confirm our theory, we labeled HeLa cells with 5-ethynyl-2'-deoxyuridine (EdU) and performed subsequent flow cytometry analysis or immunofluorescence staining. The percentage of EdU-positive HeLa cells was comparable to that in ASPM KO HeLa cells (Fig. 1 *D–H*) and siRNA-mediated ASPM knockdown HeLa cells (*SI Appendix*, Fig. S1 *C–G*). It thus seems that an ASPM deficiency has no obvious impact on S phase progression.

We next performed DNA fiber assays to determine whether ASPM has a role in replication fork dynamics. We found that the iododeoxyuridine (IdU)-tract length for individual replication forks in ASPM KO cells (Fig. 1 *I* and *J*) or ASPM knockdown cells (*SI Appendix*, Fig. S1 *H* and *I*) was comparable to that in control cells. Taken together, we conclude that ASPM is dispensable for DNA replication under unperturbed conditions.

ASPM Ensures ATR-CHK1 Activation following Replication Stress. Given that the RAD17-RFC complex loads the 9-1-1 complex onto stalled replication forks (49), we reasoned that ASPM could modulate the ATR-CHK1 activation in response to DNA replication stress. To test this, we treated ASPM KO cells and parental HeLa cells with low dose aphidicolin (APH) (1 μM), hydroxylurea (HU) (0.2 mM) or camptothecin (CPT) (0.1 μM) for 24 h. We found that ATR phosphorylation at T1989, CHK1 at S345, and RPA32 at S33 was compromised in ASPM KO cells under all conditions, but not in the parental cells (Fig. 2*A*). Cell cycle profiling revealed that, after 24 h of HU or APH treatment, the majority of ASPM KO cells were stuck in S phase with a slight slippage into G2/M phase (*SI Appendix*, Fig. S2*A*). HU-induced phosphorylation of ATR, CHK1, and RPA32 were reduced within the first 2 h after treatment in both ASPM KO cells (Fig. 2*B*) and ASPM knockdown cells (*SI Appendix*, Fig. S2*B*). ASPM encodes two major isoforms: isoform 1, which consists of 3,477 amino acids and isoform 2, which lacks exon 18 (ASPM Δ18) and consists of 1,892 amino acids. As expression of isoform 1 is very challenging, we used isoform 2 for both in vitro biochemical assays and in vivo rescue assays. Reexpression of FLAG-ASPM Δ18 in ASPM KO cells restored ATR-CHK1 activation following HU treatment (Fig. 2*C*).

HU causes a dramatic increase in exposed ssDNA in the nascent DNA strand (42), and ssDNA could be detected by BrdU foci. We found that the percentages of both BrdU foci under nondenaturing condition and RPA32 foci in γH2AX-positive cells were significantly decreased following HU treatment in both ASPM KO cells (Fig. 2 *D–G*) and ASPM knockdown cells (*SI Appendix*, Fig. S2 *C–G*). These results suggest that ASPM impacts on ssDNA formation.

Taken together, these findings suggest that ASPM ensures timely ATR-CHK1 activation in response to HU-induced DNA replication stress.

ASPM Facilitates RAD9/TopBP1 Chromatin Loading. The replacement of RFC1 by RAD17 upon replication stress transforms the RFC complex into a RAD17-RFC complex, which promotes RAD9-RAD1-HUS1 (9-1-1) complex and TopBP1 loading onto stalled replication forks and subsequent ATR-CHK1 checkpoint activation (30–32, 34, 49). Given that ASPM physically associates with the RFC complex, RAD17, and TopBP1 (Fig. 1*C*), we decided to examine whether ASPM interacts with the 9-1-1 complex. Indeed, RAD17, RAD9, and TopBP1 were all present in the FLAG-GFP-ASPM immunocomplex that we extracted from ASPM KI cells, and the interaction was enhanced upon HU treatment (Fig. 3*A*). Furthermore, these interactions were not bridged by DNA (*SI Appendix*, Fig. S3*A*).

We next sought to determine the interplay between ASPM and RAD17, RAD9, and TopBP1. The protein levels of RPA32, pRPA32(S33), RPA70, RAD9, and TopBP1, but not RAD17, in the chromatin-enriched fraction increased upon HU treatment in mock-depleted cells; these increases were abolished in both ASPM-depleted (*SI Appendix*, Fig. S3*B* and Fig. 3*B*) and ASPM KO cells (*SI Appendix*, Fig. S3*C*). Conversely, inhibiting RAD17, but not RAD9 or TopBP1 expression, reduced the HU treatment–induced increment in ASPM levels on chromatin (Fig. 3*C*).

Coimmunoprecipitation assays revealed that TopBP1 and RAD9 were present in the RAD17 immunocomplexes (Fig. 3*D*) and that TopBP1 and RAD17 in the RAD9 immunocomplexes (Fig. 3*E*) increased upon HU treatment in mock-depleted cells; this increment was abolished in ASPM-depleted cells. The HU treatment–induced increment in the HA-RAD9/FLAG-RAD17

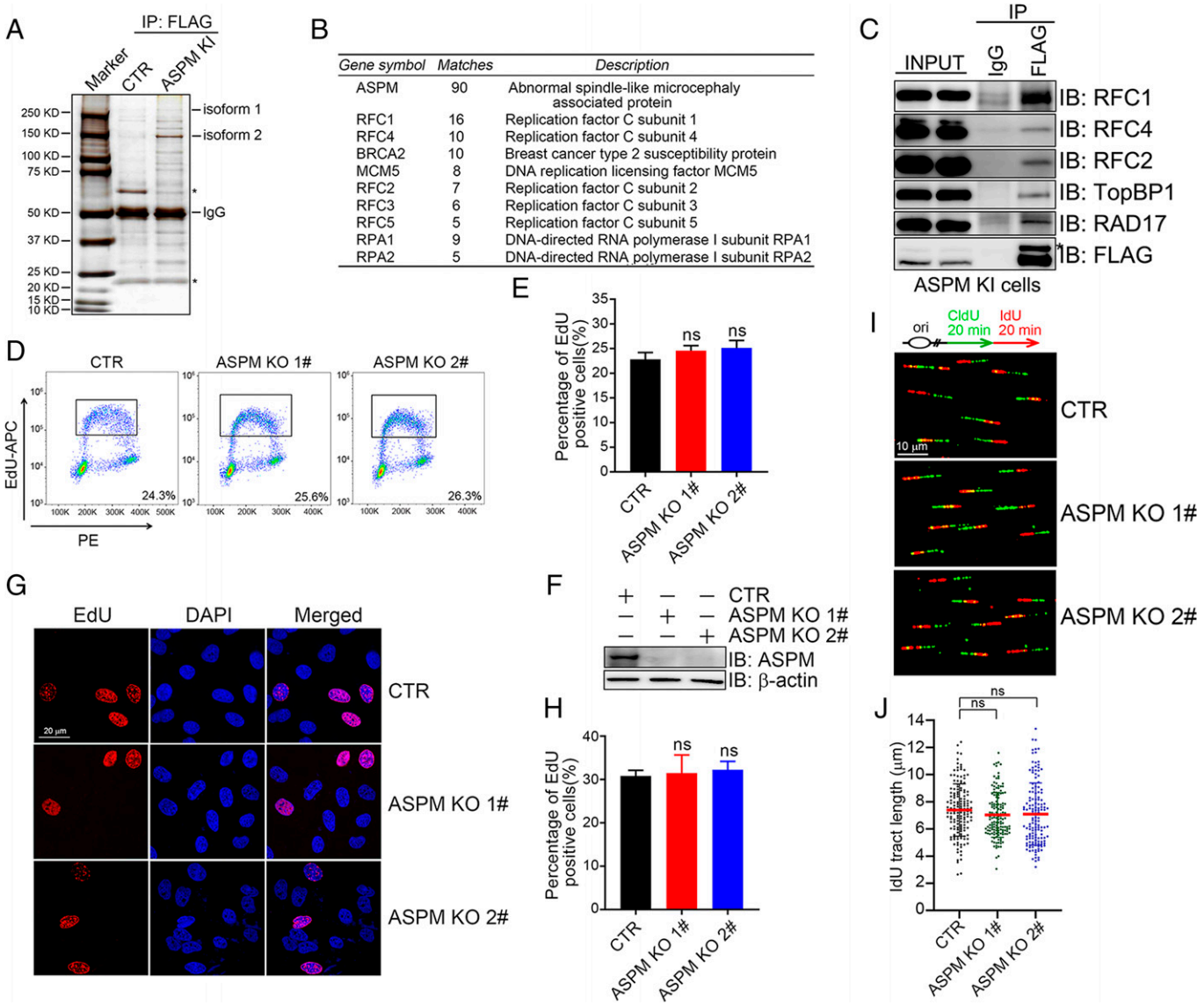

Fig. 1. ASPM associates with DNA replication factors. (*A* and *B*) Identification of ASPM-associated proteins. Control or FLAG-GFP-ASPM knockin (ASPM KI) HeLa cells were lysed and enriched using a FLAG antibody. The protein complexes were separated by SDS-PAGE and then labeled by silver staining (*A*). Proteins identified by mass spectrometric analyses are listed (*B*). (*C*) ASPM interacts with the RFC complex, RAD17, and TopBP1. HeLa cell lysates were precipitated with FLAG antibody then analyzed by immunoblotting with indicated antibodies. * in *A* and *C*: nonspecific signal. (*D–F*) ASPM is dispensable for S phase progression. ASPM KO cells were incorporated with EdU before fluorescence activated cell sorting (FACS) (*D*). The percentage of EdU-positive cells was quantified (*E*). Data represent the mean ± SEM from three independent experiments. no significance (ns), $P > 0.05$, one-way ANOVA. Loss of ASPM was analyzed by immunoblotting with indicated antibodies (*F*). (*G* and *H*) ASPM deficiency has no impact on S phase progression. ASPM KO cells were incorporated with EdU before immunofluorescence analyses (*G*). The percentage of EdU-positive cells was quantified (*H*). Data represent the mean ± SEM from three independent experiments. ns, $P > 0.05$, one-way ANOVA. (*I* and *J*) ASPM is dispensable for normal DNA replication. Representative images of CldU and IdU replication tracks (*I*) and a scatterplot of the IdU tract length for individual replication forks (*J*). Data are representative of at least three independent experiments. ns, $P > 0.05$, one-way ANOVA.

interaction in mock-depleted cells were also eliminated in ASPM-depleted cells (*SI Appendix*, Fig. S3*D*).

To explore whether ASPM serves as a scaffold protein to facilitate RAD17-dependent loading of the 9-1-1 and TopBP1 complexes on DNA, bacterially produced recombinant protein GST-RAD9 was used to pull down HIS-RAD17 or HIS-TopBP1 (1 to 290) in the absence or presence of bacterially produced ASPM Δ18 fragments (F1: 1 to 476, F2: 477 to 919, F3: 920 to 1,392, and F4: 2,941 to 3,477) (Fig. 3*F*). The interaction between GST-RAD9 and HIS-RAD17 or HIS-TopBP1 (1 to 290) was enhanced by the presence of the F1 or F2 fragment of ASPM (Fig. 3 *G* and *H*).

Finally, we found that a deficiency of pRPA32(S33) in ASPM-depleted cells in response to HU treatment was also rescued upon reexpression of FLAG-TopBP1-AAD (ATR activation domain) or FLAG-RAD9, but not by the reexpression of FLAG-RAD17 (Fig. 3*I*). Collectively, it seems that ASPM facilitates RAD17-dependent loading of RAD9 and TopBP1 onto chromatin upon replication stress.

ASPM Promotes RAD17-Dependent Loading of RAD9 and TopBP1 onto Stalled Replication Forks. We were intrigued to see that ASPM is recruited to the chromatin in response to replication stress, and so next investigated whether ASPM is precisely enriched onto the stalled replication forks. Previous isolation of proteins on nascent DNA (iPOND) proteomic screens has identified ASPM on the stalled replication forks (50, 51). Our iPOND assays found that, in ASPM KI cells, ASPM in the replication fork was barely detectable under normal conditions, yet was readily detectable upon HU treatment in the proteins

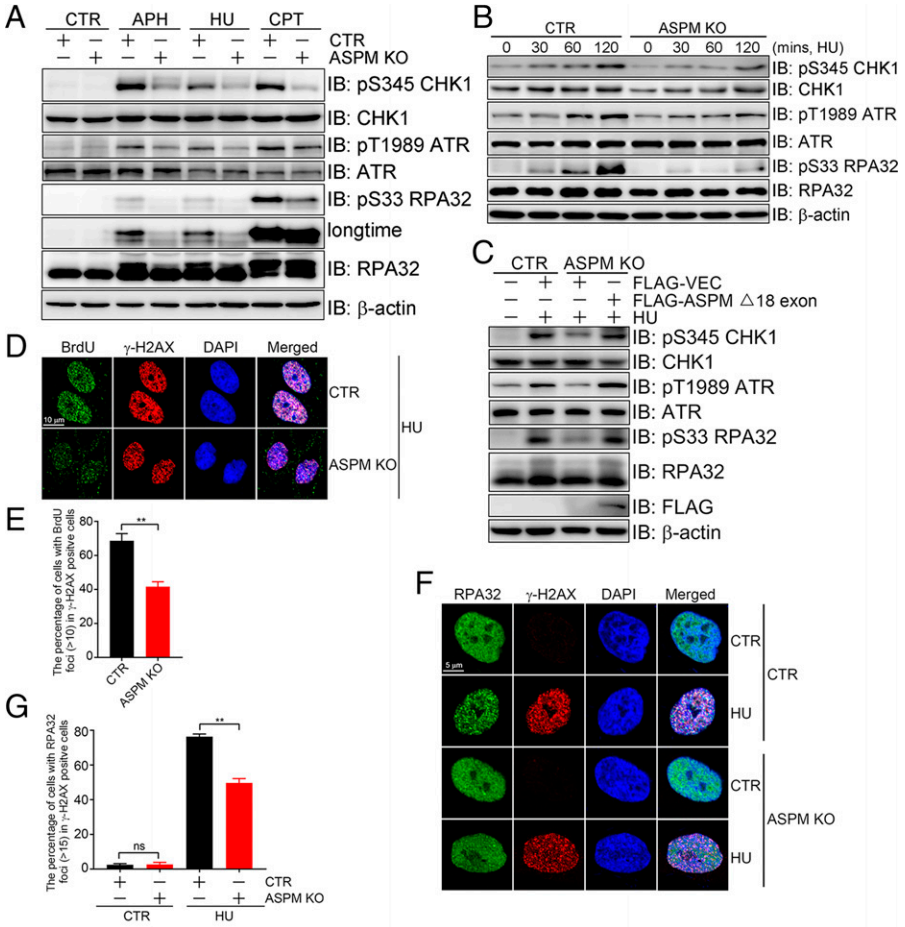

Fig. 2. ASPM ensures timely CHK1 activation following replication stress. (*A*) ASPM promotes ATR-CHK1 activation upon replication stress. Control and ASPM KO cells were incubated with low doses of APH (1 μM), HU (0.2 mM), and CPT (0.1 μM) for 24 h, followed by immunoblotting with the indicated antibodies. (*B*) ASPM promotes timely ATR-CHK1 activation upon replication stress. Control and ASPM KO cells were incubated with HU (2 mM) for the indicated times, followed by immunoblotting with the indicated antibodies. (*C*) Reexpression of FLAG-ASPM Δ18 in ASPM KO cells restored ATR-CHK1 activation upon HU treatment. Control, ASPM KO cells were transfected with FLAG-VEC or FLAG-ASPM Δ18 for 48 h and treated with HU (2 mM) for 1 h, followed by immunoblotting with the indicated antibodies. (*D*) ASPM facilitates ssDNA formation in response to replication stress. Control or ASPM KO cells were incubated with BrdU for 24 h, then treated with HU for 1 h before immunofluorescence analysis under nondenaturing conditions using the indicated antibodies. (*E*) The percentage of cells with BrdU foci (>10) in γH2AX-positive cells was quantified. Data represent the mean ± SEM from three independent experiments. $^{**}P < 0.01$, one-way ANOVA. (*F*) ASPM promotes RPA32 foci formation upon replication stress. Control or ASPM KO cells were treated with HU for 1 h, followed by immunofluorescence analysis using the indicated antibodies. (*G*) The percentage of cells with RPA32 foci (>15) in γH2AX-positive cells was quantified. Data represent the mean ± SEM from three independent experiments. $^{**}P < 0.01$; one-way ANOVA.

complexed with EdU-labeled nascent DNA and diminished upon thymidine chase (Fig. 4*A*). Proximity ligation assays (PLAs) revealed that the number of PLA foci for ASPM/EdU in cells labeled with EdU significantly increased in response to HU treatment (Fig. 4 *B* and *C*). We further found that the HU treatment–induced increment in RAD17/EdU PLA foci per positive cell in mock-depleted cells was similar to that in ASPM KO cells (Fig. 4 *D* and *E*), while RAD9/EdU and TopBP1/EdU PLA foci per positive cell in ASPM KO cells after HU treatment was significantly lower than those in mock-depleted cells (Fig. 4 *F*–*I*). Together, these data demonstrate that following HU treatment, ASPM is enriched onto stalled replication forks in a RAD17-dependent manner. This enrichment facilitates recruitment of the TopBP1 and 9-1-1 complex.

To further confirm that ASPM facilitates the recruitment of TopBP1 and the 9-1-1 complex onto replication forks in vitro, streptavidin pulldown assays showed that RPA-coated biotin-ssDNA/dsDNA was able to efficiently pull down endogenous RAD17, but not RAD9 or TopBP1, in nuclear extracts derived from ASPM KO cells. This defect was rescued by reexpression of FLAG-ASPM Δ18 (Fig. 4 *J* and *K*). Furthermore, RPA-coated and RAD17-saturated biotin-ssDNA/dsDNA was able to efficiently pull down bacterially produced GST-RAD9 and HIS-TopBP1(1-290) only in the presence of the bacterially produced F1 or F2 fragment of ASPM (Fig. 4 *L* and *M*). Taken together, these results indicate that ASPM promotes RAD17-dependent loading of RAD9 and TopBP1 onto stalled replication forks.

ASPM Protects the Nascent Strand at Stalled Replication Forks from Nucleolytic Degradation. Unprotected nascent DNA at stalled forks is at risk for nucleolytic degradation by nucleases (42). Thus far, we have seen ASPM enriched onto the stalled replication forks. To determine whether ASPM plays a role in protection of the nascent DNA strand at the stalled forks, we sequentially labeled mock-depleted, ASPM-depleted, or ASPM KO cells with chlorodeoxyuridine (CldU) and IdU for 30 min each and then treated them with HU (2 mM) for 5 h or the DNA polymerase α-inhibitor APH (5 μM) for 2 h. We found that the mean lengths of IdU tracts in both ASPM KO and ASPM knockdown cells were significantly shorter than those in control cells (Fig. 5*A* and *SI Appendix*, Fig. S4*A*). Reexpression of FLAG-ASPM Δ18 in ASPM KO cells restored ATR-CHK1 activation following HU treatment (Fig. 5*B* and *SI Appendix*, Fig. S4*B*).

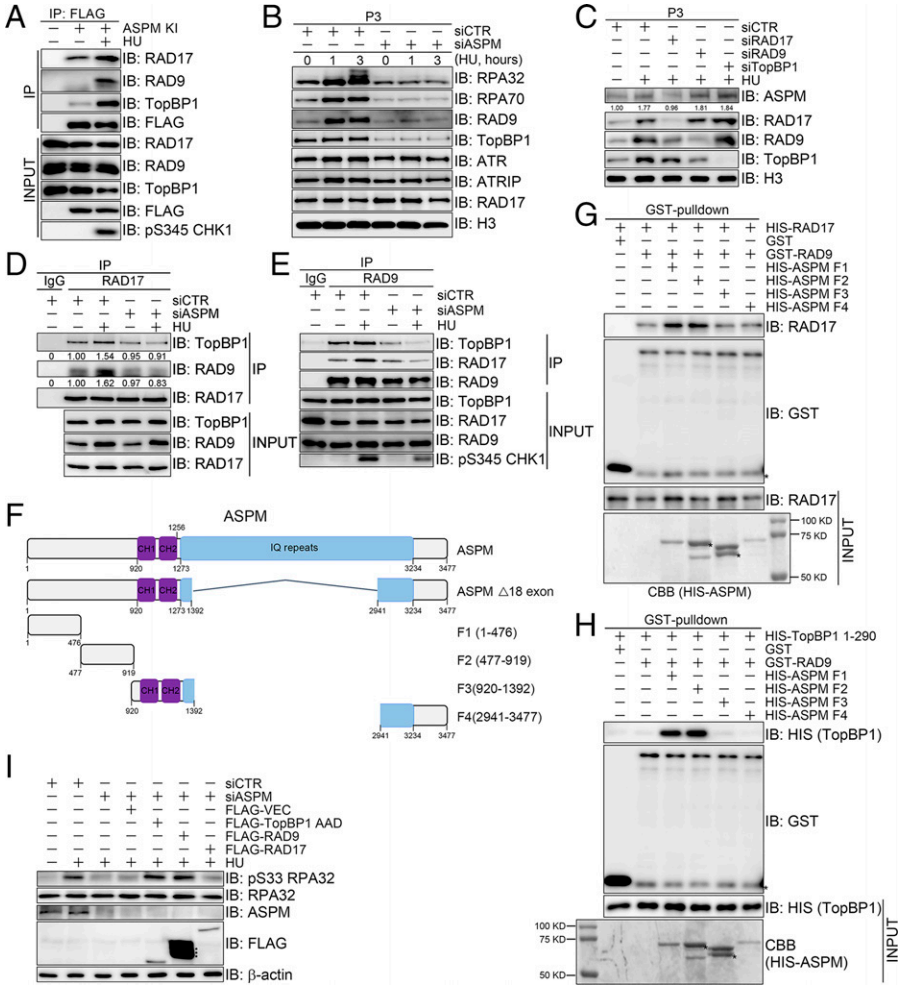

Fig. 3. ASPM facilitates RAD9/TopBP1 chromatin loading. (*A*) The associations among ASPM, RAD17, RAD9, and TopBP1 increased upon HU treatment. ASPM KI HeLa cells were treated with HU for 1 h before anti-FLAG immunoprecipitation (IP) and immunoblotting with the indicated antibodies. (*B*) ASPM promotes RAD9 and TopBP1 chromatin loading upon replication stress. Control and ASPM knockdown cells were treated with HU for the indicated times before chromatin fractionation (CF) to isolate the chromatin enriched fraction (P3) and immunoblotting with the indicated antibodies. (*C*) ASPM is enriched on chromatin in a RAD17-dependent manner. Control and RAD17, RAD9, or TopBP1 knockdown cells were treated with HU for 1 h, followed by CF to isolate the P3 fraction and immunoblotting with the indicated antibodies. (*D* and *E*) ASPM promotes the RAD17-RAD9/TopBP1 association. Control and ASPM knockdown HEK293T cells were treated with HU for 1 h before IP using RAD17 (*D*) or RAD9 (*E*) antibodies followed by immunoblotting. (*F*) The domain structure of the ASPM isoforms and fragments. (*G* and *H*) F1 and F2 ASPM fragments enhanced the interaction between GST-RAD9 and HIS-RAD17 or HIS-TopBP1 (1-290). Bacterially produced recombinant GST-RAD9 protein was used to pull down HIS-RAD17 (*G*) or HIS-TopBP1 (1-290) (*H*) in the absence or presence of bacterially produced ASPM Δ18 fragments. (*I*) Overexpression of TopBP1 or RAD9, but not RAD17, rescued the ATR activation defect caused by ASPM deficiency. HEK293T cells were first transfected with control or ASPM siRNAs for 24 h, followed by transfection with FLAG-VEC, FLAG-RAD17, FLAG-RAD9, or FLAG-TopBP1 AAD for another 48 h and then treated with HU for 1 h. Total cell lysates were extracted and subjected to immunoblotting with the indicated antibodies. * in *G*–*I*: nonspecific signal.

We obtained similar results in ASPM-depleted HeLa, U2OS, and HCT116 cells, suggesting that ASPM deficiency causes the nascent strand at stalled forks to become susceptible to nucleolytic degradation (Fig. 5*C* and *SI Appendix*, Fig. S4*C*). We also found that inhibiting ASPM expression in mouse neural progenitor cells (NPCs) using two independent shRNAs did not have a significant impact on DNA replication under normal conditions (*SI Appendix*, Fig. S4 *D* and *E*); however, nascent DNA was unprotected at the stalled replication forks, as indicated by shortened IdU track length in ASPM knockdown cells (*SI Appendix*, Fig. S4*F*). These findings indicate that like BRCA1/2, ASPM shields the nascent DNA at stalled replication forks from degradation.

Given that ASPM interacts with BRCA1 (47) and potentially with BRCA2 (Fig. 1*B*), we wanted to determine whether this role for ASPM in fork protection is independent of BRCA1/2 or not. After inhibiting BRCA1 or BRCA2 expression in control cells and ASPM KO cells, we saw no significant difference in IdU-track shortening after HU treatment (Fig. 5 *D* and *E*).

Translocase-mediated fork reversal renders nascent DNA susceptible for degradation by nucleases if protectors are absent (39, 42, 52). We thus sought to determine whether ASPM deficiency–induced nascent DNA degradation is dependent on translocases. Indeed, we found that siRNA-mediated inhibition of the translocases SMARCA1, ZRANB3, or HLTF in ASPM KO cells rescued ASPM deficiency–induced shortening of the IdU track length after HU treatment (Fig. 5 *F* and *G* and *SI Appendix*, Fig. S4*G*). Collectively, these findings demonstrate that ASPM protects nascent strand at stalled replication forks from being degraded via either the same pathway as BRCA1, or in an epistatic manner to BRCA1/2 that is dependent on fork reversal.

ASPM Protects Reversed Forks from MRE11-Mediated Degradation. Newly synthesized strands at stalled replication forks are susceptible to degradation by several nucleases, including EXO1,

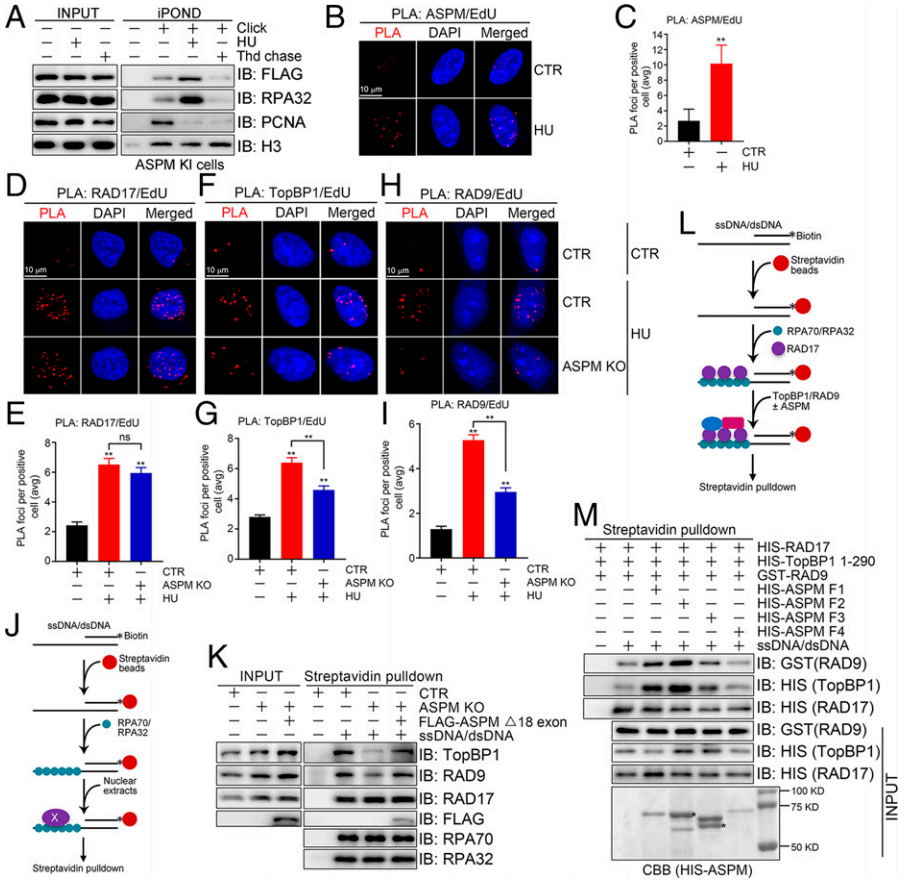

Fig. 4. ASPM promotes RAD17-dependent loading of the RAD9 and TopBP1 onto the stalled replication fork. (*A*) ASPM is recruited to stalled replication forks. HeLa cells were labeled with EdU before analysis by iPOND assay and immunoblotting with the indicated antibodies. (*B* and *C*) ASPM is enriched at stalled replication forks. HeLa cells were labeled with EdU and treated with/without HU, then subjected to PLA with anti-ASPM and anti-EdU antibodies. Representative images of PLA foci (red) (*B*) and the quantification of the average number of PLA foci per focus-positive cell (*C*) are shown. (Scale bar, 10 μm.) Data represent the mean ± SEM from three independent experiments. $^{**}P < 0.01$; one-way ANOVA. (*D* and *E*) ASPM is dispensable for RAD17 enrichment at stalled replication forks. Control and ASPM KO cells were labeled with EdU before treatment with/without HU followed by PLA with anti-RAD17 and anti-EdU antibodies. Representative images of PLA foci (red) (*D*) and the quantification of the average number of PLA foci per focus-positive cell (*E*) are shown. (Scale bar, 10 μm.) Data represent the mean ± SEM from three independent experiments. ns, $P > 0.05$; one-way ANOVA. (*F–I*) ASPM is required for TopBP1 and RAD9 enrichment at stalled replication forks. Control and ASPM KO cells were labeled with EdU before treatment with/without HU followed by PLA with anti-TopBP1, anti-RAD9, or anti-EdU antibodies. Representative images of PLA foci (red) (*F* and *H*) and the quantification of the average number of PLA foci per focus-positive cell (*G* and *I*) are shown. Data represent the mean ± SEM from three independent experiments. $^{**}P < 0.01$, one-way ANOVA. (*J* and *K*) ASPM facilitates recruitment of TopBP1 and 9-1-1 complex onto replication forks in vitro. Schematic of ssDNA/dsDNA streptavidin pulldown (*J*). Biotinylated ssDNA/dsDNA were first bound with streptavidin beads and coated with bacterially produced recombinant RPA32 and PRA70, followed by incubating with nuclear extracts derived from CTR, ASPM KO, or reexpression of FLAG-ASPM Δ18 cells (*K*). (*L* and *M*) F1 and F2 ASPM fragments promote RAD17-dependent loading of RAD9 and TopBP1 onto stalled replication forks. Schematic of ssDNA/dsDNA streptavidin pulldown (*L*). RPA-coated and RAD17-saturated biotin-ssDNA/dsDNA was used to pull down bacterially produced GST-RAD9 and HIS-TopBP1(1-290), followed by immunoblotting with the indicated antibodies (*M*). * in *M*: nonspecific signal.

DNA2, and MRE11 (42, 45, 53–55). CtIP synergizes with BRCA1, not BRCA2, to prevent DNA2-dependent overresection of nascent strands to protect reversed forks from nucleolytic degradation upon replication stress (43, 45, 46). We wanted to find out which nuclease mediates the degradation of nascent strands at stalled replication forks in ASPM-deficient cells. DNA fiber assays revealed that inhibiting EXO1 or DNA2 expression by siRNA had no obvious impact on the IdU/CldU ratio in mock-depleted cells, while the reduction in the ratio in ASPM/EXO1- or ASPM/DNA2-codepleted cells was similar to that in ASPM-depleted only cells (Fig. 6 *A–C*).

We then turned our attention to CtIP and MRE11: Here, neither inhibiting CtIP nor MRE11 expression compromised stalled fork stability (Fig. 6 *D–F*). However, inhibiting MRE11 expression, but not CtIP, rescued the ASPM deficiency–induced reduction of the IdU/CldU ratio (Fig. 6 *E* and *F*). Moreover, the number of the PLA foci of MRE11/EdU in cells labeled with EdU was significantly increased in ASPM KO cells. Thymidine chase moved the nascent, EdU-labeled DNA segment away from the replication fork. This finding suggests that ASPM suppresses MRE11 recruitment at stalled replication forks (Fig. 6 *G* and *H*). Together, we conclude that ASPM protects nascent strands from degradation by MRE11 at stalled replication forks.

ASPM Ensures Chromosome Stability in Response to Replication Stress. In our final assays, we sought to determine the biological consequences of an ASPM deficiency in response to DNA replication stress. In response to a low dose of HU (0.2 mM or 0.5 mM), the IdU/CldU ratio was significantly reduced compared to that in mock-depleted cells and further reduced in ASPM-depleted cells (Fig. 7*A*). In addition, cotreatment with APH (5 μM) and HU (2 mM) led to an increment in the percentage of stalled replication forks and a reduction in the percentage of stalled fork restart in ASPM-deficient cells (Fig. 7*B*).

Mitotic spread assays showed that, at the chromosome level, inhibiting ASPM expression by CRISPR/Cas9-mediated KO or by siRNA led to a significant increment in the total level of

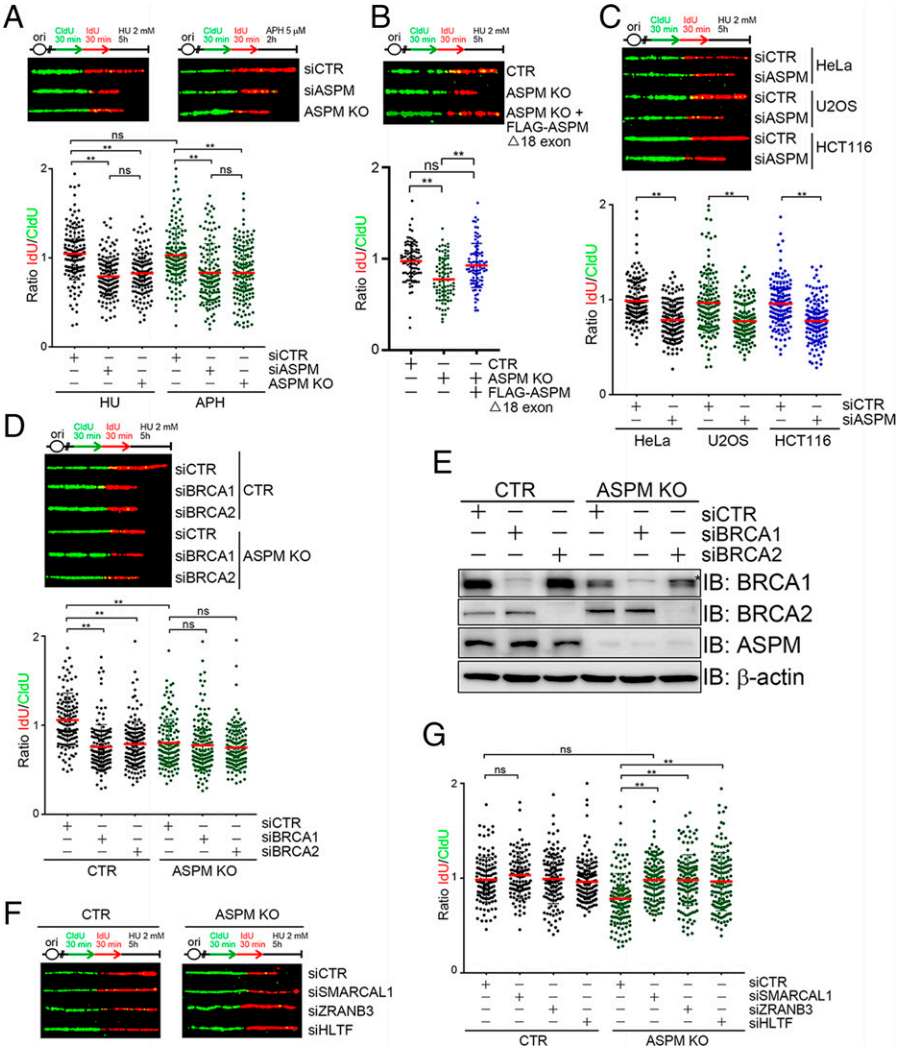

Fig. 5. ASPM protects nascent strand at stalled replication forks from nucleolytic degradation. (*A*) ASPM protects extensive nucleolytic fork degradation in response to replication stress. Control, ASPM KO, and ASPM knockdown cells were labeled sequentially with CldU and IdU for 30 min, then treated with HU (2 mM) for 5 h (*Left*) or APH (5 μM) for 2 h (*Right*), followed by conducting a DNA fiber assay. The experimental design and representative images of CldU and IdU replication tracks (*Top*) and the ratios of IdU tracks compared to CldU tracks (*Bottom*) are shown. Data are representative of at least three independent experiments. ns, $P > 0.05$, $^{**}P < 0.01$; one-way ANOVA. (*B*) Reexpression of FLAG-ASPM Δ18 in ASPM KO cells restored ATR-CHK1 activation upon HU treatment. Control, ASPM KO, or reexpression of FLAG-ASPM Δ18 cells were labeled sequentially with CldU and IdU for 30 min, then treated with HU (2 mM) for 5 h, followed by conducting a DNA fiber assay. Data represent mean ± SEM from three independent experiments. ns, $P > 0.05$; $^{**}P < 0.01$; one-way ANOVA. (*C*) Nascent DNA degradation at stalled replication forks was increased in ASPM-deficient cells. Control and siRNA-mediated ASPM knockdown HeLa, U2OS, or HCT116 cells were labeled sequentially with CldU and IdU for 30 min before HU treatment (2 mM) for 5 h and DNA fiber assay. The experimental design and representative images of CldU and IdU replication tracks (*Top*) and the ratios of IdU tracks compared to CldU tracks (*Bottom*) are shown. Data are representative of at least three independent experiments. $^{**}P < 0.01$; one-way ANOVA. (*D* and *E*) ASPM, like BRCA1/2, protects against extensive fork degradation. Control and ASPM KO HeLa cells were first transfected with siRNAs against BRCA1 or BRCA2 for 48 h before DNA fiber assay (as described in *C*). Representative images of CldU and IdU replication tracks are shown (*D*, *Top*). The ratios of IdU tracks compared to CldU tracks (*D*, *Bottom*). The effect of BRCA1 and BRCA2 knockdown was determined by immunoblotting with the indicated antibodies (*E*). Data are representative of at least three independent experiments. ns, $P > 0.05$, $^{**}P < 0.01$; one-way ANOVA. * in *E*: nonspecific signal. (*F* and *G*) ASPM-mediated protection of nascent strands at the stalled replication forks requires replication fork reversal. Measurement of nascent DNA degradation in ASPM-deficient cells following depletion of SMARCAL1, ZRANB3, or HLTF. Control or ASPM KO cells were labeled sequentially with CldU and IdU for 30 min, then treated with HU (2 mM) for 5 h before DNA fiber assay. The experimental design and representative images of CldU and IdU replication tracks (*F*) and the ratios of IdU tracks compared to CldU tracks (*G*) are shown. Data are representative of at least three independent experiments. ns, $P > 0.05$, $^{**}P < 0.01$; one-way ANOVA.

chromosome abnormalities under unperturbed conditions, in response to HU treatment (Fig. 7 *C*–*F*).

Given that high expression of ASPM has been reported in several cancer types and correlates with poor prognosis, we mined the cancer database GEPIA (gepia.cancer-pku.cn/detail.php?gene=ASPM) and found that high expression of ASPM in 9,494 cases of 33 types of cancer associates with unfavorable prognosis (Fig. 7*G*). In particular, high ASPM expression in liver hepatocellular carcinoma (*SI Appendix*, Fig. S5*A*), lung adenocarcinoma (*SI Appendix*, Fig. S5*B*), brain lower grade glioma (*SI Appendix*, Fig. S5*C*), adrenocortical carcinoma (*SI Appendix*, Fig. S5*D*), and pancreatic adenocarcinoma (*SI Appendix*, Fig. S5*E*), possesses significantly poorer overall survival. These results suggested that inhibiting ASPM expression could be a therapeutic strategy. Indeed, inhibition of ASPM expression by KO or siRNA-mediated knockdown sensitized cells to HU treatment (Fig. 7 *H* and *I*). Taken together, we conclude that ASPM is essential for maintaining chromosome stability in response to replication stress and is a potential target for therapy.

Discussion

An ASPM deficiency tips neural stem cell division from symmetric division to asymmetric division. The result is a reduction

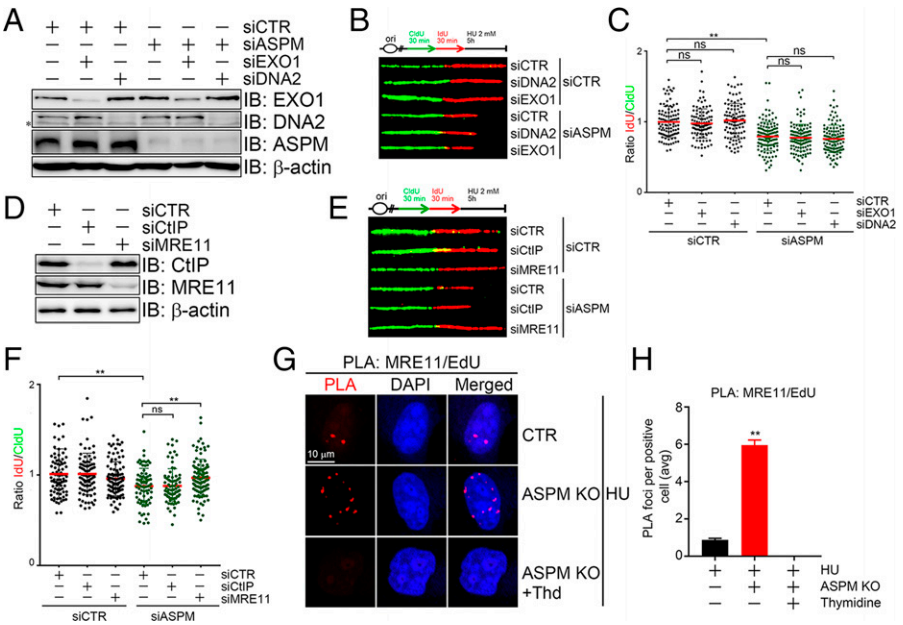

Fig. 6. ASPM protects reversed forks from MRE11-mediated degradation. (*A–C*) EXO1 and DNA2 are dispensable for fork degradation in ASPM-deficient cells. Control or ASPM KO cells were first transfected with siRNAs against EXO1 and DNA2 for 48 h, then sequentially labeled with CldU and IdU before DNA fiber assay. The knockdown effect of MRE11, CtIP, and ASPM in HeLa cells was measured by immunoblotting with the indicated antibodies (*A*). The experimental design and representative image of CldU and IdU replication tracks are shown (*B*). The ratios of the IdU track compared to the CldU track are plotted (*C*). Data are representative of at least three independent experiments. ns, $P > 0.05$, $^{**}P < 0.01$; one-way ANOVA. * in *A*: nonspecific signal. (*D–F*) MRE11 promotes extensive fork degradation in ASPM-deficient cells. Control or ASPM KO cells were first transfected with siRNAs against CtIP and MRE11 for 48 h, then sequentially labeled with CldU and IdU before DNA fiber assay. The knockdown effect of MRE11 and CtIP was measured by immunoblotting with the indicated antibodies (*D*). The experimental design and representative images of CldU and IdU replication tracks are shown (*E*). The ratios of the IdU track compared to the CldU track are plotted (*F*). Data are representative of at least three independent experiments. ns, $P > 0.05$, $^{**}P < 0.01$; one-way ANOVA. (*G* and *H*) ASPM suppresses MRE11 enrichment at stalled replication forks. Control and ASPM KO cells were labeled with EdU for 15 min, with or without 1 h thymidine (10 μM), and then treated with HU before PLA with anti-MRE11 and anti-EdU antibodies. Representative images of PLA foci (red) are shown (*G*) together with the average number of PLA foci per focus-positive cell (*H*). (Scale bar, 10 μm.) Data represent the mean ± SEM from three independent experiments. $^{**}P < 0.01$; one-way ANOVA.

in the pool of neuroprogenitor cells and thus primary microcephaly (56). Given the role of ASPM in spindle formation and homologous recombination (HR) repair of DSBs, but the uncertainty surrounding accurate genome duplication, in this study we were interested in determining whether ASPM is involved in the control of DNA replication and/or a replication stress response. Using a series of cellular models, we demonstrated that in the context of an ASPM deficiency, the ATR-CHK1 replication checkpoint fails to be activated in cancer cells as both the 9-1-1 complex and TopBP1 fail to be recruited to the stalled replication forks. As such, the stalled replication forks destabilize under conditions of replication stress both in cancer cells and neuroprogenitor cells, as the nuclease MRE11 gains access to degrade the nascent DNA exposed at the stalled forks (Fig. 8).

This mechanism may indicate an additional function of ASPM during the pathogenesis of primary microcephaly. During neurogenesis, endogenous replication stressors such as reactive oxygen species induce replication checkpoint activation and stalled replication forks; if there is an ASPM deficiency, the stalled forks can collapse and the resulting one-ended DSBs fail to be repaired. As a result, replication fails and apoptosis ensues, thus reducing the number of neuroprogenitor cells.

In addition to ASPM encoded by MCPH5, other MCPH proteins encoded by MCPH1-3, MCPH6-9, MCPH12, MCPH14, and MCPH25 control microtubule stability during cell division and/or centrosome biogenesis. We thus consider that investigations into whether these centrosome/spindle-associated MCPH proteins may possess similar functions in ATR-CHK1 activation and stabilization of stalled replication forks in response to replication stress are warranted.

Outside of microcephaly, ASPM is one of the hub genes and its high expression correlates with an unfavorable prognosis of many types of cancers (57) (Fig. 7*G*), including hepatocellular carcinoma (58–62) (*SI Appendix*, Fig. S5*A*), breast cancer (63), lung cancer (64) (*SI Appendix*, Fig. S5*B*), low grade glioma (*SI Appendix*, Fig. S5*C*), adrenocortical carcinoma (*SI Appendix*, Fig. S5*D*), and pancreatic adenocarcinoma (*SI Appendix*, Fig. S5*E*). Indeed, we now know from the data presented here that high ASPM expression would stabilize stalled replication forks, which would promote HR repair of DSBs and replication fork collapse–induced one-ended DSBs by safeguarding the BRCA1 stability (37). This mechanism could potentially drive therapeutic resistance. On the other hand, others have shown that inhibiting ASPM expression in various cancer cells (12, 47, 65–69) inhibits cell viability and proliferation and/or sensitized cells to irradiation or DNA damaging agents. Indeed, an ASPM deficiency sensitized cells to acute or chronic HU treatment (Fig. 7 *H* and *I*) (70) and pyridostatin (a G-quadruplex stabilizer) treatment (54). With these findings in mind, we consider that ASPM could serve as a promising therapeutic target for multiple cancers.

Materials and Methods

Cell Lines and Culture Conditions. Human HeLa, U2OS, and HEK293T cells were cultured in Dulbecco's modified Eagle's medium (DMEM) supplemented with 10% fetal bovine serum (FBS), penicillin, and streptomycin (1%) at 37 °C in a 5% CO_2 humidified incubator. NPCs were a kind gift from Prof. Haiyun Gan, Shenzhen Institute of Advanced Technology, Shenzhen, China. NPCs were grown in N2B27 with EGF/FGF (10 ng/mL each), on 0.2% gelatin-coated plates/flasks.

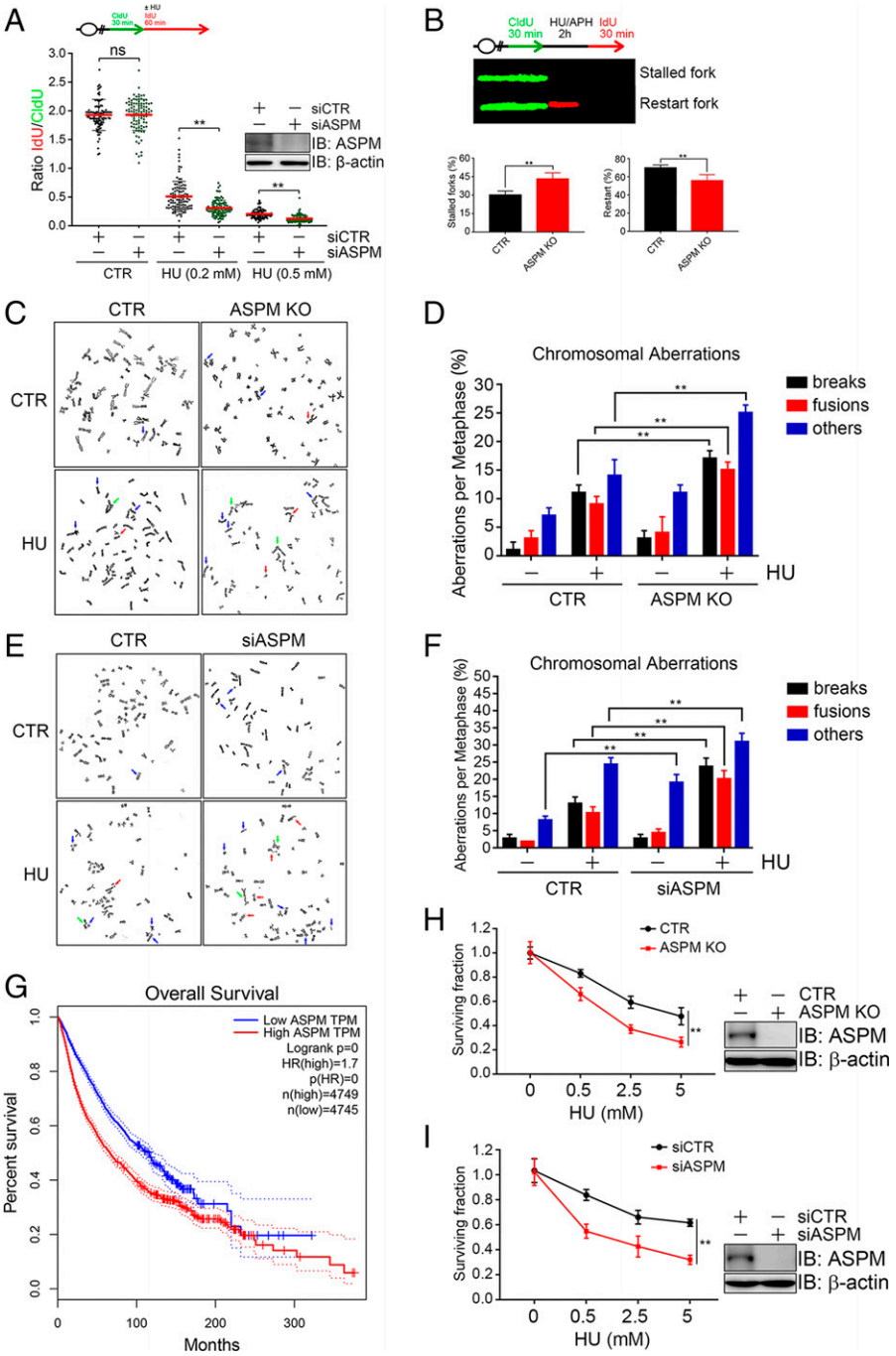

Fig. 7. ASPM ensures chromosome stability in response to replication stress. (*A*) ASPM slowed down the replication fork progression under low concentration of HU. The sketch delineates the experimental design. HeLa cells were first labeled with CldU for 30 min and then incubated with IdU and low dose of HU for 1 h. The ratios of IdU track compared to CldU track were plotted. Data are representative of at least three independent experiments. ns, $P > 0.05$, $^{**}P < 0.01$; one-way ANOVA. (*B*) ASPM was required for restart of stalled replication forks. HeLa cells were first labeled with CldU for 30 min, then treated with HU (2 mM) and APH (5 mM) for 2 h, followed by IdU labeling for another 30 min. Cells were harvested and subjected to DNA fiber assay. *Top*: Schematic of the DNA fiber experiment and representative image of CldU and IdU replication tracks. *Bottom*: The percentage of stalled fork and restart forks was quantified. Data represent the mean ± SEM from three independent experiments. $^{**}P < 0.01$; one-way ANOVA. (*C*–*F*) Control, ASPM KO, or siRNA-mediated ASPM knockdown HeLa cells were exposed to HU (2 mM) for 12 h followed by colchicine treatment. The cells were harvested for metaphase spread assay. More than 100 mitotic chromosomes were randomly analyzed. Representative metaphase spreads (*C* and *E*) and the percentages of spreads containing aberrant chromosomal structures (breaks, fusions, and others) are shown in *D* and *F*. Data represent the mean ± SEM from three independent experiments. $^{**}P < 0.01$; one-way ANOVA. The arrows indicate chromosome aberrations. (*G*) The total survival plots of high ASPM expression of 33 cancer types, n(high) = 4,749, n(low) = 4,745. The survival plots of ASPM are present in this weblink: gepia.cancer-pku.cn/detail.php?gene=ASPM. (*H* and *I*) ASPM was required for cell survival upon HU treatment. Control, ASPM KO, or ASPM knockdown HeLa cells were exposed to different dosages of HU for 24 h followed by continued growth for 14 d. The colonies were stained with crystal violet and the clonogenic efficiency was calculated. The KO and knockdown effects were measured by immunoblotting with indicated antibodies. Data represent the mean ± SEM from three independent experiments. $^{**}P < 0.01$; one-way ANOVA.

Transient Transfection. Transient transfection to overexpress plasmids in cell lines was carried out using polyethylenimine (PFI, Polyscience), according to the manufacturer's instructions. siRNAs were transiently transfected using Lipofectamine RNAiMAX transfection reagent (Invitrogen), according to the manufacturer's instructions. All siRNA sequences are listed in *SI Appendix*, Table S1.

ASPM KI and ASPM KO Cell Line Generation. Both KO and KI cell lines were generated using CRISPR-Cas9 genome-editing technology. For the ASPM KI, a single guide RNA (sgRNA) was designed in front of the start codon ATG within the ASPM first exon. The sgRNA (TCGAATCTGCCATGGCGAAC)-containing PX458 (Addgene, 48138) plasmid was cotransfected with pDsRed-FLAG-GFP

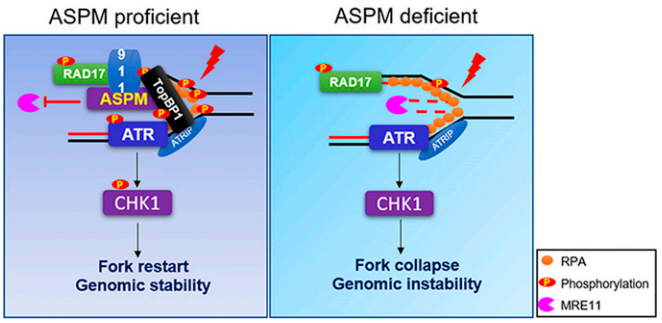

Fig. 8. Working model. *Left*: ASPM proficient. In response to replication stress, RAD17 and ATR-ATRIP are first recruited to the stalled fork in a ssDNA-dependent manner. RAD17 recruits ASPM to the stalled replication fork, which in turn facilities TopBP1 and 9-1-1 loading to promote ATR-CHK1 activation. On the other hand, ASPM antagonizes MRE11 loading onto the stalled replication fork, which protects nascent DNA from degradation to promote fork restart and genomic maintenance. *Right*: ASPM deficient. In the absent of ASPM, TopBP1 and 9-1-1 loading is compromised and fails to activate the ATR-CHK1 kinase cascade. Moreover, excessive MRE11 loading will degrade nascent DNA, resulting in replication fork collapse and genomic instability.

donor plasmids (800 bp around the DSB site) into HeLa cells. After 48 h, both GFP- and RFP-positive single cells were selected by flow cytometry, diluted to single clones, and then confirmed by PCR and sequencing. For the ASPM KO, the sgRNA (GGCCCTAGACAACCCTAACG)-containing PX459 (Addgene, 48139) plasmid was transfected into HeLa cells. After 48 h, the cells were subcloned into 96-well plates after drug selection in the presence of 1 μg/mL puromycin for 24 h.

Immunoblotting. Cell lysates were prepared in 6× SDS (sodium dodecyl sulfate) loading buffer (62.5 mM Tris·HCl, pH 6.8, 2% sodium dodecyl sulfate, 0.05% bromophenol blue, 20% glycerol, 5% β-mercaptoethanol) and boiled for 5 to 10 min. Lysates were separated by SDS-PAGE (polyacrylamide gel electrophoresis) and transferred to polyvinylidene fluoride membranes (Roche) before blocking with skim milk and then blotting with the indicated antibodies (*SI Appendix*, Table S2). Primary antibodies were incubated overnight at 4 °C while secondary antibodies were incubated for 1 h at room temperature. A Super Signal West Femto Substrate kit was used to visualize proteins after processing membranes using a FUJIFILM imaging system.

Chromatin Fractionation. Cells were collected by trypsinization and suspended with buffer A (10 mM Hepes pH 7.9, 0.34 M sucrose, 20% glycerol, 1 mM dithiothreitol [DTT], 10 mM KCl, 1.5 mM $MgCl_2$) and 0.1% Triton X-100. The soluble cytoplasmic fraction (S2) was obtained after the first addition of buffer A. The remaining nuclear fraction was washed with buffer A (without 0.1% Triton X-100) before buffer B (30 mM ethylenediaminetetraacetic acid (EDTA), 0.2 mM ethylene glycol tetraacetic acid (EGTA), and 1 mM dithiothreitol (DTT)) was added to the cells and kept on ice for 10 min. The soluble nuclear fraction was separated by centrifuge and the insoluble chromatin fraction was washed with buffer B by centrifugation at 13,000 × *g* relative centrifugal force for 1 min at 4 °C. Cell fractions were collected in the respective sample buffers before analysis by immunoblotting.

Immunoprecipitation. HEK293T cells were collected by trypsinization and washed with phosphate-buffered solution (PBS) (precooled) twice. The cells were lysed in NETN buffer (0/150/400 mM NaCl, 20 mM Tris·HCl [pH 7.5], 0.5% Nonidet P-40, 5 mM EDTA) with protease inhibitor for 30 min. The supernatants were incubated with a primary antibody at 4 °C overnight. Then, protein A/G Sepharose beads were used to capture the primary antibody-bound proteins for 1 h at 4 °C. The beads were washed three to five times in NETN buffer before being transferred to the appropriate sample buffer, and analyzed by immunoblotting.

Immunofluorescence. U2OS or HeLa cells were grown on top of coverslips and then fixed with 4% paraformaldehyde (PFA) for 10 min. The cells were washed with PBS twice and then permeabilized with 0.5% Triton X-100 (in PBS) for 5 min. The cells were blocked with 2% bovine serum albumin (BSA) (in 0.1% PBS with Tween-20 (PBST)) for 30 to 60 min before being incubated with primary and then secondary antibodies for 1 h each at room temperature (RT). The nuclei were stained with DAPI for 2 min and then images were captured under a DragonFly confocal imaging system (Andor).

DNA Fiber Assay. Cells were labeled with 40 μM CldU for 30 min, followed by 100 μM IdU for another 30 min prior to incubation with/without the indicated drugs. Cells were harvested by trypsinization followed by the cell mixture (labeled cells: nonlabeled cells=1:1) loaded onto a slide and cell lysis solution (200 mM Tris·HCl, pH 7.5, 50 mM EDTA and 0.5% SDS) added. After air drying, the fibers were fixed in methanol:acetic acid (3:1) solution and denatured in 2.5 N HCl. Then, the slides were washed twice with 1× PBS and then blocked with 2% BSA (in PBS) before the addition of anti-BrdU primary and suitable secondary antibodies. Images were captured under a DragonFly confocal imaging system (Andor).

iPOND. Cells were labeled with 10 μM EdU for 15 min before treatment or not with the indicated drugs. The cells were then fixed with 1% PFA for 20 min at RT and then the cross-links were quenched with 1.25 M glycine for 5 min using a table concentrator. Next, the cells were collected and permeated in permeabilization buffer for 30 min on ice. Before the next step, a click chemistry reaction was prepared to conjugate biotin to EdU. After rinsing with PBS, the nuclei were subjected to the click reaction with 10 μM biotin-azide for 1.5 h at 4 °C under rotation, followed by washes with PBS and resuspension in cell lysis buffer (1% SDS in 50 mM Tris·HCl, PH 8.0). Then, the cells were sonicated for 10 min at high intensity (1 s/5 s on/off pulses) to obtain 100- to 300-bp fragments. Streptavidin-conjugated Dynabeads M-280 (Invitrogen) were added to the fragments and incubated at 4 °C overnight. Finally, the samples were washed twice with lysis buffer and then washing buffer (containing 500 mM NaCl) before analysis by immunoblotting.

PLA Assay. Cells were first labeled with 10 μM EdU for 15 min at 37 °C, with or without a 1-h thymidine (10 μM) chase, and then subjected to a 4-mM HU treatment for 3 h prior to two washes with PBS. The cells were fixed with 3.7% formaldehyde for 10 min, then permeabilized with 0.2% Triton X-100 for 5 min and blocked with 2% BSA for 1 h. Next, the cells were incubated with two primary antibodies at 4 °C overnight. The subsequent procedures were carried out according to the manufacturer's instructions of the Duolink In Situ Red Starter kit (Sigma-Aldrich). Images were captured using a DragonFly confocal imaging system (Andor).

Metaphase Spreads. For metaphase enrichment, growing cultures were incubated with 0.4 μg/mL of the spindle poison cochicine (Sigma, catalog #C3915) at 37 °C for 4 h. The cells were then harvested using trypsin before 0.075 M KCl was added and left to incubate at 37 °C for 15 min to allow the cells to swell. Then, 1 mL Carnoy's fixatives (methanol:glacial acetic acid 3:1) were slowly added while gently mixing by pipetting. Additional Carnoy's fixatives were added and the cells were resuspended for fixation for 10 min at RT. These steps were repeated two additional times, and the cells were incubated overnight during the fixation. The supernatant was discarded each time. The fixed cells were gently resuspended and the cell densities were optimized onto a precleaned slide. The slides were stained with Giemsa at 37 °C for 3 min, then rinsed with deionized water and air dried. The slides were scanned and images were captured under the DragonFly confocal imaging system (Andor).

Colony Formation Assay. Cells were collected by trypsinization and counted such that 150 to 300 cells were added to each well of a six-well plate. The cells were treated with the indicated drugs after 24 h. The cells were cultured for a further 12 to 15 d. Then, the cells were fixed with 4% PFA before 1× crystal violet staining at RT for 15 min.

BrdU Labeling. BrdU incorporation was performed as previous described (47).

ssDNA/dsDNA Pull-Down Assay. To generate ssDNA/dsDNA, biotinylated DNA oligomers (5′-AACCTGTCGTGCCAGCTGCA-biotin-3′) were first annealed to complementary ssDNA (5′-TGCAGCTGGCACGACAGGTTTTAATGAATCGGCCAACGCGCGGGGAGAGGCGGTTTGCGTATTGGGCGCTCTTCCGCTTCGCAGCGAGTC-3′) with molar ratio 1:4. The annealed ssDNA/dsDNA product (100 pmol) was first bound with streptavidin-M280 beads (Thermo Fisher), followed by extensive washing with binding buffer (10 mM Tris·HCl [pH 7.5], 100 mM NaCl, 10% glycerol, 0.01%

Nonidet P-40, and BSA 10 mg/mL) and then coated with bacterially produced recombinant RPA32 and PRA70 (~1 μg). After extensive washing with binding buffer, the beads carrying RPA-ssDNA/dsDNA were incubated in nuclear extracts or bacterially produced recombinant HIS-TopBP1, GST-RAD9 for 30 min, followed by extensive washing with NETN buffer three times. The proteins bound to beads were then subjected to immunoblotting.

Statistical Analyses. All statistical analyses were performed in Microsoft Excel and GraphPad Prism 8. If the data conformed to a normal distribution, unpaired *t* tests were used, or a one-way analysis of variance (ANOVA) when comparing more than two samples. Each experiment was repeated at least three times. In all cases, $P < 0.05$ was considered to indicate a statistically significant difference.

Data, Materials, and Software Availability. All study data are included in the article and/or supporting information.

ACKNOWLEDGMENTS. We would like to thank all members of the X.X. laboratory for their help and useful discussions, Prof. Haiyun Gan at Shenzhen Institute of Advanced Technology for providing the mouse neuroprogenitor cells, and Prof. Jiadong Wang from Peking University for the expression construct of FLAG-TopBP1 AAD. This work was supported by the National Natural Science Foundation of China grants 32090031, 31761133012, and 31530016; the 973 projects 2017YFA0503900; the Natural Science Foundation of Guangdong 2020A1515010422; and the Shenzhen Science and Technology Innovation Commission projects JCYJ 201805073000163, JCYJ20180507182049853, and JCYJ20170412113009742.

1. X. Zhou, Y. Zhi, J. Yu, D. Xu, The Yin and Yang of autosomal recessive primary microcephaly genes: Insights from neurogenesis and carcinogenesis. *Int. J. Mol. Sci.* **21**, E1691 (2020).
2. A. M. Kaindl *et al.*, Many roads lead to primary autosomal recessive microcephaly. *Prog. Neurobiol.* **90**, 363–383 (2010).
3. S. Xu, X. Wu, B. Peng, S.-L. Cao, X. Xu, Primary microcephaly with an unstable genome. *Genome Instability & Disease* **1**, 235–264 (2020).
4. M. Naveed *et al.*, Comprehensive review on the molecular genetics of autosomal recessive primary microcephaly (MCPH). *Genet. Res.* **100**, e7 (2018).
5. X. Xu, J. Lee, D. F. Stern, Microcephalin is a DNA damage response protein involved in regulation of CHK1 and BRCA1. *J. Biol. Chem.* **279**, 34091–34094 (2004).
6. S. Y. Lin, R. Rai, K. Li, Z. X. Xu, S. J. Elledge, BRIT1/MCPH1 is a DNA damage responsive protein that regulates the Brca1-Chk1 pathway, implicating checkpoint dysfunction in microcephaly. *Proc. Natl. Acad. Sci. U.S.A.* **102**, 15105–15109 (2005).
7. P. Létard *et al.*, Autosomal recessive primary microcephaly due to ASPM mutations: An update. *Hum. Mutat.* **39**, 319–332 (2018).
8. M. Gai *et al.*, ASPM and CITK regulate spindle orientation by affecting the dynamics of astral microtubules. *EMBO Rep.* **17**, 1396–1409 (2016).
9. X. Zhong, L. Liu, A. Zhao, G. P. Pfeifer, X. Xu, The abnormal spindle-like, microcephaly-associated (ASPM) gene encodes a centrosomal protein. *Cell Cycle* **4**, 1227–1229 (2005).
10. K. Jiang *et al.*, Microtubule minus-end regulation at spindle poles by an ASPM-katanin complex. *Nat. Cell Biol.* **19**, 480–492 (2017).
11. X. L. Xu *et al.*, The microtubule-associated protein ASPM regulates spindle assembly and meiotic progression in mouse oocytes. *PLoS One* **7**, e49303 (2012).
12. V. C. Pai *et al.*, ASPM promotes prostate cancer stemness and progression by augmenting Wnt-Dvl-3-β-catenin signaling. *Oncogene* **38**, 1340–1353 (2019).
13. J. J. Buchman, O. Durak, L. H. Tsai, ASPM regulates Wnt signaling pathway activity in the developing brain. *Genes Dev.* **25**, 1909–1914 (2011).
14. P. S. Tsegay, Y. Lai, Y. Liu, Replication stress and consequential instability of the genome and epigenome. *Molecules* **24**, E3870 (2019).
15. M. K. Zeman, K. A. Cimprich, Causes and consequences of replication stress. *Nat. Cell Biol.* **16**, 2–9 (2014).
16. Y. Chen, J. Yuan, The post translational modification of key regulators of ATR signaling in DNA replication. *Genome Instability & Disease* **2**, 92–101 (2021).
17. Y. Cui, S. S. Palii, C. L. Innes, R. S. Paules, Depletion of ATR selectively sensitizes ATM-deficient human mammary epithelial cells to ionizing radiation and DNA-damaging agents. *Cell Cycle* **13**, 3541–3550 (2014).
18. R. M. Williams, L. A. Yates, X. Zhang, Structures and regulations of ATM and ATR, master kinases in genome integrity. *Curr. Opin. Struct. Biol.* **61**, 98–105 (2020).
19. A. Maréchal, L. Zou, DNA damage sensing by the ATM and ATR kinases. *Cold Spring Harb. Perspect. Biol.* **5**, a012716 (2013).
20. Z. Guo, A. Kumagai, S. X. Wang, W. G. Dunphy, Requirement for Atr in phosphorylation of Chk1 and cell cycle regulation in response to DNA replication blocks and UV-damaged DNA in Xenopus egg extracts. *Genes Dev.* **14**, 2745–2756 (2000).
21. E. Petermann, K. W. Caldecott, Evidence that the ATR/Chk1 pathway maintains normal replication fork progression during unperturbed S phase. *Cell Cycle* **5**, 2203–2209 (2006).
22. R. L. Flynn, L. Zou, ATR: A master conductor of cellular responses to DNA replication stress. *Trends Biochem. Sci.* **36**, 133–140 (2011).
23. D. R. Iyer, N. Rhind, The intra-S checkpoint responses to DNA damage. *Genes (Basel)* **8**, E74 (2017).
24. S. Rundle, A. Bradbury, Y. Drew, N. J. Curtin, Targeting the ATR-CHK1 axis in cancer therapy. *Cancers (Basel)* **9**, E41 (2017).
25. H.-W. Hsiao, C.-C. Yang, H. Masai, Roles of Claspin in regulation of DNA replication, replication stress responses and oncogenesis in human cells. *Genome Instability & Disease* **2**, 263–280 (2021).
26. Y. Zou, Y. Liu, X. Wu, S. M. Shell, Functions of human replication protein A (RPA): From DNA replication to DNA damage and stress responses. *J. Cell. Physiol.* **208**, 267–273 (2006).
27. J. Fan, N. P. Pavletich, Structure and conformational change of a replication protein A heterotrimer bound to ssDNA. *Genes Dev.* **26**, 2337–2347 (2012).
28. Y. Fukumoto, M. Ikeuchi, Y. Nakayama, N. Yamaguchi, The KYxxL motif in Rad17 protein is essential for the interaction with the 9-1-1 complex. *Biochem. Biophys. Res. Commun.* **477**, 982–987 (2016).
29. C. S. Eichinger, S. Jentsch, 9-1-1: PCNA's specialized cousin. *Trends Biochem. Sci.* **36**, 563–568 (2011).
30. L. Zou, D. Liu, S. J. Elledge, Replication protein A-mediated recruitment and activation of Rad17 complexes. *Proc. Natl. Acad. Sci. U.S.A.* **100**, 13827–13832 (2003).
31. H. L. Ball, J. S. Myers, D. Cortez, ATRIP binding to replication protein A-single-stranded DNA promotes ATR-ATRIP localization but is dispensable for Chk1 phosphorylation. *Mol. Biol. Cell* **16**, 2372–2381 (2005).
32. S. Liu *et al.*, ATR autophosphorylation as a molecular switch for checkpoint activation. *Mol. Cell* **43**, 192–202 (2011).
33. V. Ellison, B. Stillman, Biochemical characterization of DNA damage checkpoint complexes: Clamp loader and clamp complexes with specificity for 5′ recessed DNA. *PLoS Biol.* **1**, E33 (2003).
34. A. Kumagai, J. Lee, H. Y. Yoo, W. G. Dunphy, TopBP1 activates the ATR-ATRIP complex. *Cell* **124**, 943–955 (2006).
35. E. Ohashi, Y. Takeishi, S. Ueda, T. Tsurimoto, Interaction between Rad9-Hus1-Rad1 and TopBP1 activates ATR-ATRIP and promotes TopBP1 recruitment to sites of UV-damage. *DNA Repair (Amst.)* **21**, 1–11 (2014).
36. B. Michel, A. K. Sinha, D. R. F. Leach, Replication fork breakage and restart in *Escherichia coli*. *Microbiol. Mol. Biol. R* **82,** e00013 (2018).
37. C. J. Ma, B. Gibb, Y. Kwon, P. Sung, E. C. Greene, Protein dynamics of human RPA and RAD51 on ssDNA during assembly and disassembly of the RAD51 filament. *Nucleic Acids Res.* **45**, 749–761 (2017).
38. M. Berti *et al.*, Sequential role of RAD51 paralog complexes in replication fork remodeling and restart. *Nat. Commun.* **11**, 3531 (2020).
39. R. Bétous *et al.*, Substrate-selective repair and restart of replication forks by DNA translocases. *Cell Rep.* **3**, 1958–1969 (2013).
40. G. M. Weaver, K. A. Mettrick, T. A. Corocher, A. Graham, I. Grainge, Replication fork collapse at a protein-DNA roadblock leads to fork reversal, promoted by the RecQ helicase. *Mol. Microbiol.* **111**, 455–472 (2019).
41. F. B. Couch *et al.*, ATR phosphorylates SMARCAL1 to prevent replication fork collapse. *Genes Dev.* **27**, 1610–1623 (2013).
42. M. Berti, D. Cortez, M. Lopes, The plasticity of DNA replication forks in response to clinically relevant genotoxic stress. *Nat. Rev. Mol. Cell Biol.* **21**, 633–651 (2020).
43. A. Taglialatela *et al.*, Restoration of replication fork stability in BRCA1- and BRCA2-deficient cells by inactivation of SNF2-family fork remodelers. *Mol. Cell* **68**, 414–430.e8 (2017).
44. D. Lemaçon *et al.*, MRE11 and EXO1 nucleases degrade reversed forks and elicit MUS81-dependent fork rescue in BRCA2-deficient cells. *Nat. Commun.* **8**, 860 (2017).
45. K. Schlacher *et al.*, Double-strand break repair-independent role for BRCA2 in blocking stalled replication fork degradation by MRE11. *Cell* **145**, 529–542 (2011).
46. S. Przetocka *et al.*, CtIP-mediated fork protection synergizes with BRCA1 to suppress genomic instability upon DNA replication stress. *Mol. Cell* **72**, 568–582.e6 (2018).
47. S. Xu *et al.*, ASPM promotes homologous recombination-mediated DNA repair by safeguarding BRCA1 stability. *iScience* **24**, 102534 (2021).
48. M. S. Kang *et al.*, Regulation of PCNA cycling on replicating DNA by RFC and RFC-like complexes. *Nat. Commun.* **10**, 2420 (2019).
49. J. Lee, W. G. Dunphy, Rad17 plays a central role in establishment of the interaction between TopBP1 and the Rad9-Hus1-Rad1 complex at stalled replication forks. *Mol. Biol. Cell* **21**, 926–935 (2010).
50. H. Dungrawala *et al.*, The replication checkpoint prevents two types of fork collapse without regulating replisome stability. *Mol. Cell* **59**, 998–1010 (2015).
51. C. Alabert *et al.*, Nascent chromatin capture proteomics determines chromatin dynamics during DNA replication and identifies unknown fork components. *Nat. Cell Biol.* **16**, 281–293 (2014).
52. A. C. Kile *et al.*, HLTF's ancient HIRAN domain binds 3′ DNA ends to drive replication fork reversal. *Mol. Cell* **58**, 1090–1100 (2015).
53. S. Mijic *et al.*, Replication fork reversal triggers fork degradation in BRCA2-defective cells. *Nat. Commun.* **8**, 859 (2017).
54. K. Schlacher, H. Wu, M. Jasin, A distinct replication fork protection pathway connects Fanconi anemia tumor suppressors to RAD51-BRCA1/2. *Cancer Cell* **22**, 106–116 (2012).
55. A. M. Kolinjivadi *et al.*, Smarcal1-mediated fork reversal triggers Mre11-dependent degradation of nascent DNA in the absence of Brca2 and Stable Rad51 nucleofilaments. *Mol. Cell* **67**, 867–881.e7 (2017).
56. M. R. Capecchi, A. Pozner, ASPM regulates symmetric stem cell division by tuning Cyclin E ubiquitination. *Nat. Commun.* **6**, 8763 (2015).
57. J. M. Xue, Y. Liu, L. H. Wan, Y. X. Zhu, Comprehensive analysis of differential gene expression to identify common gene signatures in multiple cancers. *Med. Sci. Monit.* **26**, e919953 (2020).
58. Z. Yang *et al.*, CCNB2, CDC20, AURKA, TOP2A, MELK, NCAPG, KIF20A, UBE2C, PRC1, and ASPM may be potential therapeutic targets for hepatocellular carcinoma using integrated bioinformatic analysis. *Int. J. Gen. Med.* **14**, 10185–10194 (2021).
59. D. Chen *et al.*, Bioinformatic evidence reveals that cell cycle correlated genes drive the communication between tumor cells and the tumor microenvironment and impact the outcomes of hepatocellular carcinoma. *BioMed Res. Int.* **2021**, 4092635 (2021).
60. S. Zhang, R. Peng, R. Xin, X. Shen, J. Zheng, Conjoint analysis for hepatic carcinoma with hub genes and multi-slice spiral CT. *Medicine (Baltimore)* **99**, e23099 (2020).
61. Z. Zhou *et al.*, Screening hub genes as prognostic biomarkers of hepatocellular carcinoma by bioinformatics analysis. *Cell Transplant.* **28**(1_suppl.)76S–86S (2019).
62. Y. Zeng *et al.*, *CCNB2*, *TOP2A*, and *ASPM* reflect the prognosis of hepatocellular carcinoma, as determined by weighted gene coexpression network analysis. *BioMed Res. Int.* **2020**, 4612158 (2020).
63. G. Chen *et al.*, Identification of candidate biomarkers correlated with poor prognosis of breast cancer based on bioinformatics analysis. *Bioengineered* **12**, 5149–5161 (2021).

64. K. Wang *et al.*, Identification of differentially expressed genes in non-small cell lung cancer. *Aging (Albany NY)* **11**, 11170–11185 (2019).
65. T. A. Kato, R. Okayasu, P. A. Jeggo, A. Fujimori, ASPM influences DNA double-strand break repair and represents a potential target for radiotherapy. *Int. J. Radiat. Biol.* **87**, 1189–1195 (2011).
66. W. J. Zeng *et al.*, Aberrant ASPM expression mediated by transcriptional regulation of FoxM1 promotes the progression of gliomas. *J. Cell. Mol. Med.* **24**, 9613–9626 (2020).
67. L. Wang *et al.*, ASPM facilitates colorectal cancer cells migration and invasion by enhancing β-catenin expression and nuclear translocation. *Kaohsiung J. Med. Sci.* **38**, 129–138 (2022).
68. B. Wu, C. Hu, L. Kong, ASPM combined with KIF11 promotes the malignant progression of hepatocellular carcinoma via the Wnt/β-catenin signaling pathway. *Exp. Ther. Med.* **22**, 1154 (2021).
69. H. Zhang *et al.*, ASPM promotes hepatocellular carcinoma progression by activating Wnt/β-catenin signaling through antagonizing autophagy-mediated Dvl2 degradation. *FEBS Open Bio* **11**, 2784–2799 (2021).
70. M. Olivieri *et al.*, A genetic map of the response to DNA damage in human cells. *Cell* **182**, 481–496.e21 (2020).